JOURNAL OF GEOPHYSICAL RESEARCH, VOL. 112, C05025, doi:10.1029/2005JC003364, 2007

Circulation and water mass transformation in a model of the Chukchi Sea

Michael A. Spall[1]

Received 24 October 2005; revised 11 January 2007; accepted 23 March 2007; published 11 May 2007.

[1] The circulation and water mass transformation in a regional ocean-ice model of the Chukchi Sea are discussed. The model has horizontal resolution of $O(4$ km), is forced by fluxes derived from daily NCEP reanalysis fields, and has seasonally varying transport, temperature, and salinity imposed at Bering Strait. Many of the observed characteristics of the mean circulation and seasonal cycle in the Chukchi Sea are reproduced. The discussion focuses on: the branching of the inflow transport into pathways following Herald Canyon, Central Channel, and the Alaskan coast; the pattern of ice melt; and the water mass transformation and formation of winter water and hypersaline water. The ice melt pattern and timing is strongly influenced by advection through Bering Strait. High frequency forcing results in a larger region of ice melt, particularly over the shoals and in the northern Chukchi Sea, compared to monthly mean forcing. In the model, the seasonal cycle of salinity in the southern and central Chukchi Sea is dominated by advection through Bering Strait, while local atmospheric forcing and brine rejection are more important north of Herald and Hanna Shoals and in Barrow Canyon. However, since the residence time in the Chukchi Sea is generally less than 1 year, interannual variability in the Bering Strait salinity will be reflected in the salinity across the Chukchi Sea and at Barrow Canyon.

Citation: Spall, M. A. (2007), Circulation and water mass transformation in a model of the Chukchi Sea, *J. Geophys. Res.*, *112*, C05025, doi:10.1029/2005JC003364.

1. Introduction

[2] Waters flowing into the Arctic Ocean from the Pacific Ocean must pass through Bering Strait and across the broad, O (800 km), and shallow, O(50 m), Chukchi Sea. The annual mean transport of approximately 0.8 Sv (1 Sv = 10^6 m^3 s^{-1} [*Roach et al.*, 1995; *Woodgate et al.*, 2005a, hereinafter W05a]) is northward from the Pacific Ocean into the Arctic Ocean. There is a strong seasonal cycle, with maximum transport in summer, although strong wind events prevalent in winter can force high frequency fluctuations and even reversals in the flow. There is also a seasonal cycle in temperature and salinity, reflecting warming and ice melt in the Bering Sea in summer and freezing and brine rejection in winter. This flux of heat, fresh water, and nutrients through Bering Strait have a significant effect on the thermohaline properties of the Arctic Ocean and result in enhanced biological productivity within the Chukchi Sea [*Walsh et al.*, 1989]. The Pacific Waters fluxed through Bering Strait play an important role in the maintenance of the Arctic halocline [*Steele et al.*, 2001], which shields the ice-covered interior of the Arctic from the warm, salty waters of Atlantic origin.

[3] The circulation pathways across the Chukchi Sea are not well known, but a clearer picture is emerging. Early studies identified the fresh, warm Alaskan Coastal Current as a major transport pathway in the eastern Chukchi Sea [*Paquette and Bourke*, 1974; *Coachman et al.*, 1975]. Direct measurements [*Woodgate et al.*, 2005b, hereinafter W05b; *Weingartner et al.*, 2005] and patterns of ice melt [*Martin and Drucker*, 1997] have helped to identify two additional branches, one through Herald Canyon and one between Herald Shoal and Hannah Shoal, called the Central Channel flow. All of these pathways appear to be significant, with transports of $O(0.2-0.4$ Sv) each. There is also significant exchange through Long Strait between the coast of Siberia and Wrangle Island. Approximately 0.1 Sv of water is carried in the Siberian Coastal Current from the northwest through Long Strait, although interannual variability is large and the Siberian Coastal Current is not present every year. The net flow through this passage is less than this because there is often a flow in the opposite direction offshore of the Siberian Coastal Current [*Weingartner et al.*, 1998]. Short term current meter [*Johnson*, 1989] and ADCP [*Münchow et al.*, 2000] measurements indicate eastward transport along the upper shelf break north of Hannah Shoal, in opposite direction to the local mean wind. *Weingartner et al.* [2005] suggest that at least some of this water flowed northwards through the Central Channel, and that, further to the east, it merges with the northeastward flowing Alaskan Coastal Current and Alaskan Coastal Water at the head of Barrow Canyon, increasing the transport through Barrow Canyon beyond what is carried directly from Bering Strait along the Alaskan coast. Despite these recent advances, measurements in the Chukchi Sea remain sparse,

[1]Department of Physical Oceanography, Woods Hole Oceanographic Institution, Woods Hole, Massachusetts, USA.

0148-0227/07/2005JC003364$09.00

and the pathways, residence times, and water mass transformations that take place within the Chukchi Sea are difficult to discern from observations alone.

[4] Several modeling studies have been used to explore the circulation within the Chukchi Sea. The early studies of *Overland and Roach* [1987] and *Spaulding et al.* [1987] identified the meridional sea surface height gradient as the driving mechanism for the flow through Bering Strait. *Proshutinsky* [1986] applied a low resolution model to the circulation within the Chukchi Sea and found two branches of flow, one along the Alaskan Coast and another to the northwest. *Winsor and Chapman* [2004] found in a barotropic, high resolution model that the flow across the Chukchi Sea was not well described by three distinct branches, but instead was more of a single, basin-wide current system. There are high resolution baroclinic models with ice that extend over the whole Arctic Ocean [e.g., *Maslowski and Lipscomb*, 2003], but the analysis of such models has not focused on the Chukchi Sea. However, Clement et al. (2005) did use one such model to study the circulation in the Bering Sea and the exchange through Bering Strait with the Chukchi Sea.

[5] The model used here is high resolution, baroclinic, has realistic forcing, and thermodynamically and dynamically active sea-ice. The main intent of this study is to demonstrate that the regional model reproduces the essential characteristics of the circulation and seasonal cycle within the Chukchi Sea, and to diagnose the relative influences of local versus remote (Bering Strait) forcing for the seasonal cycle in circulation, temperature, salinity, and ice cover.

2. Model Configuration and Forcing

[6] The model used in this study is the hydrostatic version of the MIT primitive equation model [*Marshall et al.*, 1997]. The model solves momentum, temperature, and salinity equations using level (depth) coordinates in the vertical and a staggered C-grid in the horizontal. The nonlinear equation of state of *Jackett and McDougall* [1995] is used to calculate density from temperature and salinity. The model has a free surface and uses a partial cell treatment for accurate representation of bottom topography and horizontal pressure gradients.

[7] Subgridscale mixing is parameterized by biharmonic diffusion and viscosity in the horizontal (coefficients 10^8 m^4 s^{-1}) and second order diffusion and viscosity in the vertical (coefficients 10^{-4} m^2 s^{-1}). There is a quadratic bottom drag with coefficient 10^{-3}. The results are not overly sensitive to small variations in these coefficients. The model also employs the KPP mixing parameterization [*Large et al.*, 1994] in the vertical to represent mixing due to shear instabilities and convective instability.

[8] The ocean circulation model is coupled to an ice model with thermodynamics that simulate ice thickness and concentration, based on the 2-category model of *Hibler* [1980]. Snow is simulated as in *Zhang et al.* [1998] by assuming that, if the atmospheric temperature is below freezing, precipitation is snow and the surface albedo is that of snow instead of ice. The albedo is gradually changed back to that of wet or dry ice (depending on if there is sufficient heat flux to form melt pools) for snow thickness less than 0.15 m. The Hibler 2-category model and its variants use a so-called zero-layer thermodynamic model to estimate ice growth and decay. The zero-layer thermodynamic model assumes that ice does not store heat and, therefore, tends to exaggerate the seasonal variability in ice thickness. The ice model dynamics are viscous-plastic [*Hibler*, 1979], making use of the alternating-direction-implicit method of *Zhang and Rothrock* [2000]. For details, the reader is referred to the MITgcm web page (http://mitgcm.org, sea ice package).

[9] The model is forced with surface heat flux, fresh water flux, and momentum fluxes. All forcing fields are obtained from the daily NCEP reanalysis product (NCEP Reanalysis data provided by the NOAA-CIRES Climate Diagnostics Center, Boulder, Colorado, USA, from their Web site at http://www.cdc.noaa.gov). The sensible and latent heat fluxes are derived from atmospheric 10 m winds, 2 m atmospheric temperature and specific humidity using the bulk formulae of *Large and Pond* [1981, 1982]. The downward longwave and shortwave radiation and precipitation are also specified, while the outgoing longwave radiation is calculated from the surface temperature. The surface momentum flux is derived from the atmospheric winds.

[10] The model is initialized at rest with a vertical profile of temperature and salinity from the January mean Polar Science Center Hydrographic Climatology (PHC3.0, updated from *Steele et al.* [2001]) taken at 210°E, 74°N. The circulation in the Chukchi Sea is not sensitive to the initial conditions for integration times greater than approximately 1 year. Typical residence times in the Chukchi Sea are 6 months (discussed further below). The initial ice thickness is set to 2 m everywhere, and the model integration begins on January 1, 2000. The model is run for a period of three years, repeating the daily forcing from year 2000 in each model year. The repeat annual forcing is used so that any long-term trends can be attributed to spin-up and not changes in the forcing. The analysis in this paper is from the third year, although results from the second year are similar.

[11] The model is configured on a spherical grid with grid spacing of 0.05° in latitude and 0.1° in longitude. This corresponds to approximately 5 km in latitude and 4 km in longitude within the Chukchi Sea. There are 12 levels in the vertical with thicknesses of 10 m, 10 m, 15 m, 15 m, 20 m, 30 m, 40 m, 50 m, 80 m, 150 m, 250 m, and 330m. The vertical resolution is highest in the upper water column and, given the present focus on the Chukchi Sea, the model extends down to only 1000 m. There are at most 4 model levels over most of the Chukchi Sea.

[12] The bottom topography is derived from the International Bathymetric Chart of the Arctic Ocean (IBCAO) with native resolution of 1 minute in latitude and longitude, interpolated to the model grid. The model domain extends 40° in longitude from 180°W to 140°W and 11° in latitude from 66°N to 77°N (Figure 1, contours to 75 m depth only). The model boundaries are vertical walls with no slip and no flux boundary conditions. A channel has been implemented that connects the shelf-slope region at the eastern end of the model domain to the Bering Strait. This is done in order to force a transport through Bering Strait and conserve mass in the domain while avoiding the use of open boundary conditions, which can lead to some non-physical results and difficulties with flow and tracers being advected out of the domain. Model calculations have been carried out

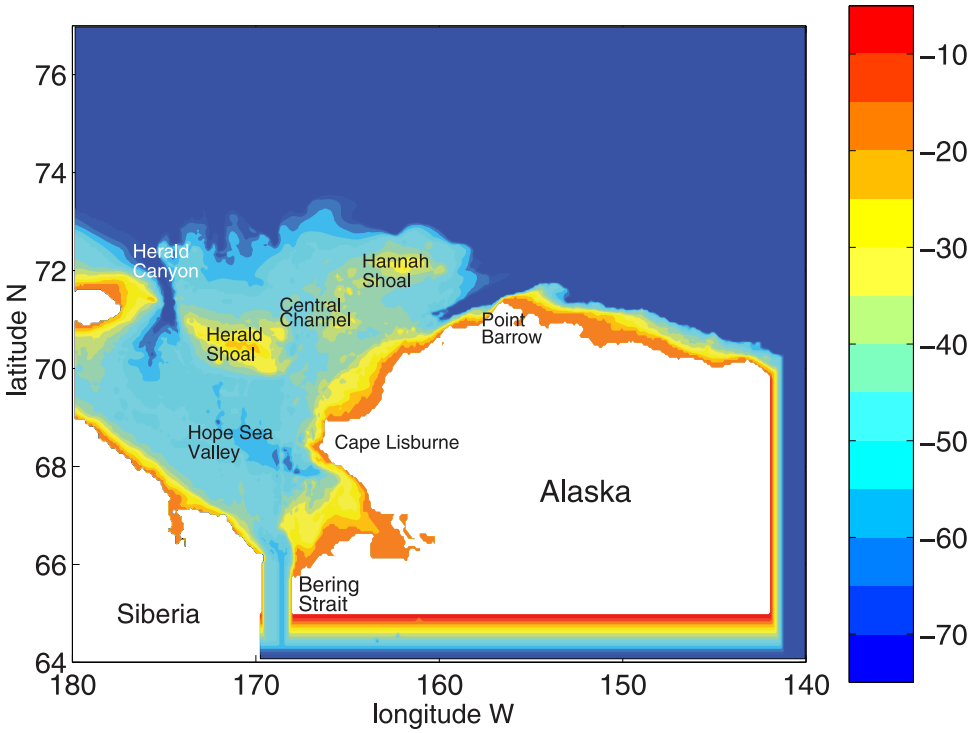

Figure 1. Basin configuration and bottom topography, major geographic features are labeled (contoured to 75 m, contour interval 5 m).

in a domain that extends 10° further to the east, and with the northern boundary at 74°N, and the results within the Chukchi Sea are essentially identical to those for the standard domain.

[13] There is a strong seasonal cycle of transport and property fluxes through the Bering Strait and into the Chukchi Sea (W05a). This is forced in the model by restoring terms in the momentum, temperature, and salinity equations that are active only within the strait between latitudes 65°N and 66°N. The model fields are strongly restored (timescale 1 hour) towards specified values that vary in both space and time to reflect the observed climatological fluxes within Bering Strait. The resulting mass flux through Bering Strait is provided by transport from the eastern slope region through the channel.

[14] The restoring functions for temperature and salinity are derived from the observations of W05a. A seasonal cycle in temperature and salinity is imposed throughout the water column, and a warm, fresh surface layer is also provided in summer. The Alaskan Coastal Current is represented by a warm, fresh surface trapped layer near the eastern boundary of Bering Strait. The analytic functions for temperature and salinity, are

$$T(x,z,t) = \max\left(-1.8, T_0 + e^{z/H_s}\,(T_{acc}A(x) + T_s)B(t) + \Delta T\,\sin\left(2\pi\frac{t-\phi}{\Phi}\right)\right), \quad (1)$$

$$S(x,z,t) = S_0 + e^{z/H_s}\,(S_{acc}A(x) + S_s)B(t) + \Delta S\,\sin\left(2\pi\frac{t'-\phi_S}{\Phi}\right). \quad (2)$$

The space and time functions are defined as

$$A(x) = 1 + \tanh\left(\frac{x-x_0}{L_{acc}}\right) \quad (3)$$

$$B(t) = 0.125\left[1 + \sin\left(2\pi\frac{t-\phi}{\Phi}\right)\right]^3 \quad (4)$$

The spatial function $A(x)$ defines the ACC and the time function $B(t)$ results in significant contribution for only about 5 months per year centered around day 270, set by ϕ = 150 days and Φ = 365 days. The maximum function in (1) is used to ensure that the inflowing temperature does not go below freezing. The first term on the right hand side represents the warming in the ACC and the second term is a summer surface warming that is applied uniformly across the Bering Strait. Each of these terms is attenuated with depth over vertical scale H_s. The final term introduces the seasonal cycle in temperature throughout the water column and across the strait. For temperature, the ACC is represented by a warming of T_{acc} = 3°C and a width of L_{acc} = 0.15° degrees longitude (7 km) centered at x_0 = 168.4°W [*Woodgate and Aagaard*, 2005]. The summer warming near the surface has strength T_s = 2°C with a vertical decay scale of H_s = 30 m. The seasonal cycle in temperature is ΔT = 3°C with T_0 = −0.75°C.

[15] The salinity function is similar to that for temperature. The ACC has a maximum anomaly of S_{acc} = −2.5 psu, with a surface freshening in summer of S_s = −0.5 psu [*Woodgate and Aagaard*, 2005] and a seasonal cycle for the inflow of ΔS = 0.75 psu with a mean of S_0 = 32.5 psu. The phase lag for salinity is ϕ_S = 45 days, giving the maximum

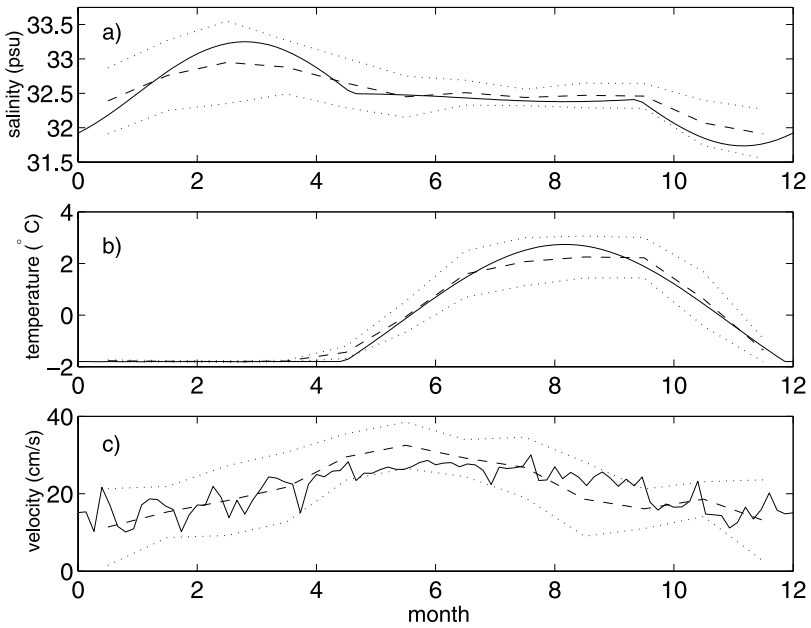

Figure 2. Properties at the mid-point of Bering Strait at 65.8°N and 42.5 m depth every 4 days in the final year of model calculation (solid lines) for (a) salinity, (b) temperature, and (c) velocity. The monthly climatology compiled by *Woodgate et al.* [2005a] is given by the dashed lines with one standard deviation indicated by the dotted lines.

salinity in early May. The time parameter $t' = t$ for $0 < t < 138$ days, $t' = 138$ for $138 < t < 282$ days, and $t' = t - 144$ for $t > 282$ days in each year.

[16] The model salinity and temperature at 65.8°N, 169°W (in Bering Strait) at 42.5 m depth are compared to the seasonal climatology of W05a in Figures 2a and 2b. The peak salinity was chosen to be higher in the model than in the observations because of the smoothing that occurs in the climatology as a result of interannual variability in the timing of the peak salinity inflow, which lowers the maximum average salinity and broadens the time period of high salinity inflow.

[17] The velocity field is restored towards a spatially uniform value with a mean of 33 cm s^{-1} and a sinusoidal seasonal cycle of amplitude 10 cm s^{-1}. The phase is such that it gives the maximum inflow in June. The inflow does not reach this specified value, however, because of the no-slip boundary conditions, bottom drag, and the winds that act to reduce the inflow. The resulting inflow velocity is shown in Figure 2c, along with the mooring climatology of W05a. The model peak occurs a little later in the year, and the seasonal cycle is somewhat less than found in the climatology. The high frequency variability in the model is a result of synoptic variability in the surface winds over the Chukchi Sea. Calculations with the monthly mean wind forcing do not produce this high frequency variability in the inflow velocity. The fluctuations are $O(10)$ cm s^{-1}, much less than is observed in the mooring data, where flow reversals are often found in winter when the mean is weak and the wind events can be very strong.

[18] The transport into the Chukchi Sea through Bering Strait for the final year of integration is shown in Figure 3. The seasonal cycle is clear, with a maximum transport of O(1.1 Sv) in summer and a minimum transport of O(0.4 Sv) in winter. The mean transport of 0.76 Sv is close to the estimated inflow transport of 0.8 Sv by *Roach et al.* [1995] and W05a. There are also fluctuations in transport as large as 0.5 Sv with timescales of days to weeks, although they are not sufficiently strong to reverse the flow.

[19] The Alaskan Coastal Current is imposed as a narrow region of warm, fresh water along the eastern boundary of Bering Strait primarily during summer and fall. A zonal section of temperature, salinity, and velocity at 65.8°N on year day 228 (mid-August) is shown in Figure 4. The ACC is evident by the warm (10°C), fresh (29 psu) region near the eastern boundary. The velocity is somewhat enhanced over that in the interior (≈40 cm s^{-1}), although it is much

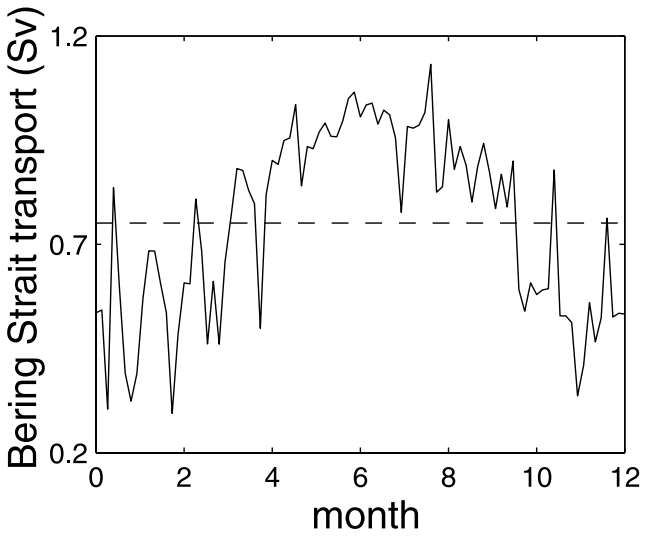

Figure 3. Inflow transport at Bering Strait for the final year of model integration (data every 4 days), mean is 0.76 Sv, dashed line, (1 Sv = 10^6 m^3 s^{-1}).

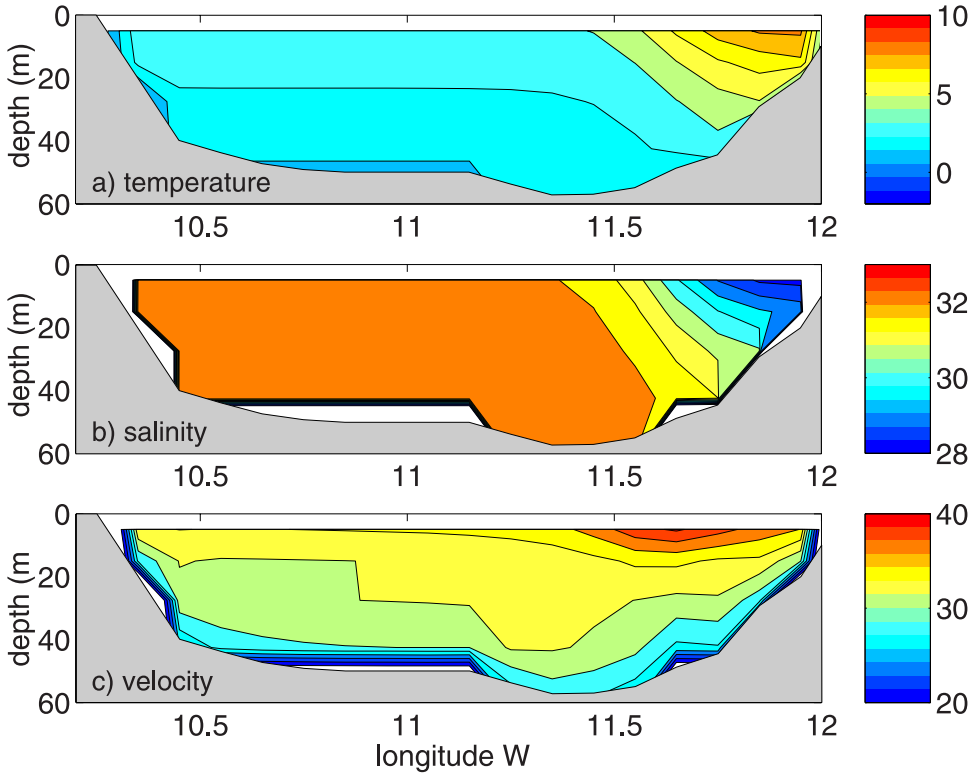

Figure 4. Zonal sections of (a) temperature (°C), (b) salinity (psu), and (c) northward velocity (cm/s) in Bering Strait at 65.8°N on model day 228 (mid-August) showing the Alaskan Coastal Current.

less than the maximum synoptic observations that can exceed 1 m s^{-1} [*Woodgate and Aagaard*, 2005], probably due to model resolution and the manner in which the model is forced in Bering Strait.

3. Comparison With Observations

[20] The model has been run for a period of three years; analysis is based on the final year of integration. A general discussion of the circulation and some comparisons with observations are carried out in this section. Interpretations of the driving mechanisms for the circulation, water mass transformation, and ice coverage are presented in the following section.

3.1. Mean Circulation

[21] The mean, depth averaged transport stream function for year 3 is shown in Figure 5 along with the bottom topography (to 75 m depth). The transport through the Chukchi Sea is carried in three main branches, as inferred from observations [*Weingartner et al.*, 1998, 2005; W05b]. In the model, the strongest branch of approximately 0.4 Sv flows through Herald Canyon, while approximately 0.2 Sv passes through the Central Channel and 0.2 Sv flows along the eastern coast. These transport estimates are close to those obtained from mooring data. The Central Channel transport is estimated to be 0.2 Sv by *Weingartner et al.* [2005], while W05b estimate the transport through Herald Canyon to be 0.28 Sv (with 0.06 Sv error bars) and the near-coastal transport off Cape Lisburne to be 0.16 Sv (with 0.04 Sv error bars). The flow recirculates anticyclonically around Hannah Shoal, with eastward transport on the northern flank and westward transport on the southern flank of the shoal. Eastward flow, in opposite direction to the local wind, has been observed north of Hannah Shoal by a 4 day current meter measurement [*Johnson*, 1989] and in synoptic ADCP [*Münchow et al.*, 2000] data. The model's eastward flow in the northern Chukchi Sea merges with the near coastal circulation at the head of Barrow Canyon, consistent with the analysis of *Weingartner et al.* [2005]. The circulation along the Siberian coast is generally weak and variable in the model, however, since Long Strait is closed, the model does not have the Siberian Coastal Current, which is forced from the northwest. Although the mean transport towards the northwest through Long Strait is estimated to be O(0.1 Sv), this is at least partially compensated for by a southeastward transport of comparable value near the coast, resulting in very little net transport [*Weingartner et al.*, 1998; W05b]. However, it is likely that there is a resulting net heat and freshwater flux into the Chukchi Sea that is missing in the model. The mean flow in the model is clearly steered by the bottom topography, and largely avoids the major topographic features of Herald and Hannah Shoals. This pattern is consistent with the notion that Taylor columns develop over the shallow topography [*Martin and Drucker*, 1997].

[22] The lack of flow over the shoals differs from the results of *Winsor and Chapman* [2004], who found a less distinct branching of the currents with some mean flow going over Herald and Hannah Shoals in a barotropic model. Calculations with their model and no bottom drag still resulted with flow over the shoals (P. Winsor, private communication). Calculations with the present model and an

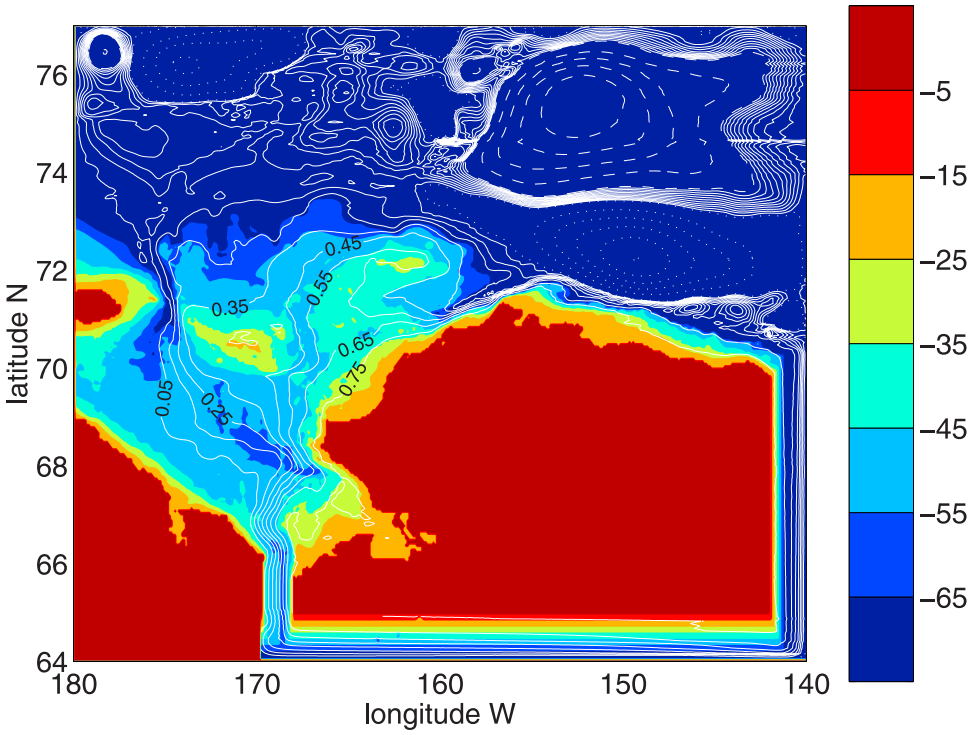

Figure 5. Mean transport stream function Ψ (Sv, 1 Sv = 10^6 m^3 s^{-1}, white contours, solid for $0 < \Psi < 1$ contour interval 0.1; dashed for $\Psi > 1$, dotted for $\Psi < 0$ contour interval 1) over bottom topography (contoured to 75 m).

increased bottom drag result in a larger fraction of the inflowing transport passing through Herald Canyon, and the overall transport is reduced, but the mean circulation still avoids Herald and Hannah Shoals. The reasons for this discrepency with the model of Winsor and Chapman are not clear.

[23] In the model, 70% of the transport through Bering Strait eventually passes along the steep topography of eastern Barrow Canyon. The maximum model annual mean transport through Barrow Canyon of 0.54 Sv is found at 156°W. This is much larger than the estimate of 0.14 ± 0.03 Sv by W05b. This observational estimate is based on a one year time series from a single current meter MK1 located at 159°41.9′W (Table 1), upstream of the maximum transport in the model. At 160°W, the transport in the model is 0.40 Sv, still more than W05b, but less than the model maximum. The transport in the model increases to the east because some of the transport that passed through the

Table 1. Mooring Data Plotted in Figure 7, Taken From *Woodgate et al.* [2005b] (W05b), *Weingartner et al.* [1998] (W98), and *Weingartner et al.* [2005] (W05)[a]

Name	Location	Speed, cm/s	Direction, °T	Source	Region, Date
MA1	65°54′ 169°25.7′	29.1	27	W05b	Bering Strait, 1990–1991
MA2	65°46.5′ 168°35.2′	28.7	8	W05b	Bering Strait, 1990–1991
MA3*	66°17.6′ 168°57.9′	22.4	338	W05b	Bering Strait, 1990–1991
MC1	67°56.9′ 174°33.2′	1.2	9	W05b	Central Chukchi, 1990–1991
MC2	68°20.5′ 172°29.8′	4.5	327	W05b	Central Chukchi, 1990–1991
MC3	68°36.7′ 171°4.4′	5.2	320	W05b	Central Chukchi, 1990–1991
MC4*	68°51.4′ 169°35.6′	5.4	331	W05b	Central Chukchi, 1990–1991
MC6	69°1.1′ 166°57.3′	4.1	6	W05b	Central Chukchi, 1990–1991
MF1	71°6.9′ 175°43.9′	0.4	337	W05b	Herald Canyon, 1990–1991
MF2*	70°57.8′ 174°11.2′	12.5	358	W05b	Herald Canyon, 1990–1991
MK1*	71°2′ 159°41.9′	14.4	74	W05b	Barrow Canyon, 1990–1991
BSN7	66°17.7′ 168°58.7′	20.4	335	W98	Bering Strait, 1991–1992
CLE3	69°1′ 166°57.5′	3.0	345	W98	Cape Lisburne, 1991–1992
HS	70°39.7′ 167°1.6′	8.2	350	W98	Central Valley, 1991–1992
UBC3*	71°3.1′ 159°32.8′	20.2	60	W98	Barrow Canyon, 1991–1992
MBC18	71°19.9′ 158°9.9′	20.6	60	W98	Barrow Canyon, 1991–1992
C1-94	70°37′ 167°5.1′	8.7	359	W05	Central Chukchi, 1994–1995
C2-93	71°16.7′ 164°16.4′	3.9	70	W05	Central Chukchi, 1993–1994
C3	71°41.1′ 167°11.4′	5.4	27	W05	Central Chukchi, 1994–1995
AC2	70°45′ 163°17.5′	5	70	W05	ACC, 1994–1995
MA3-93*	68°9′ 168°56.6′	2.9	241	W05	Central Chukchi, 1993–1994

[a]The asterisks indicate those moorings whose temperature and salinity are compared with the model in Figure 11.

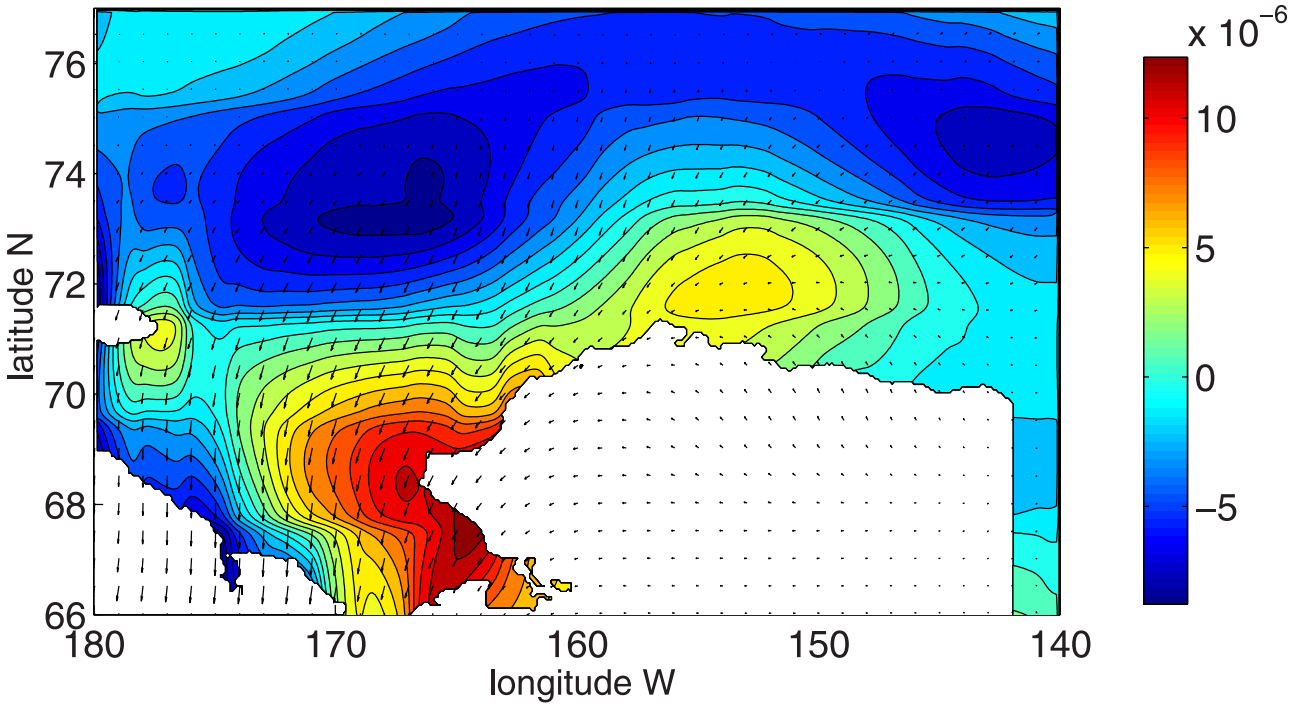

Figure 6. Annual mean wind vectors (every tenth vector) and wind curl (colors), units s^{-1} from daily NCEP winds for the year 2000. Anticyclonic curl is found over most of the Beaufort Sea with cyclonic curl near the Alaskan coast and southern Chukchi Sea.

Central Channel and Herald Canyon has flowed along the shelf break and enters Barrow Canyon along the topography from the west, as inferred from observations by *Weingartner et al.* [2005]. T. Weingartner (personal communication) used six years of current meter data (from 1990–1996) combined with ADCP data to estimate the mean transport at the location of the W05b mooring to be 0.3 Sv. This estimate is twice as large as that from 1990–1991 by W05b, but still 25% less than that found in the model. In this reconstruction, the annual mean transport varied between 0.2 Sv and 0.4 Sv, with the years 1990–1991 and 1993–1994 having the lowest annual means.

[24] Although it is difficult to compare the model mean transport with transport estimates based on point measurements from different years, the model transport is on the high end of the observational estimates. It is possible that the transport through Barrow Canyon in the model is too strong and that the offshore transport upstream (west) of Barrow Canyon into the Arctic Ocean in the model is too weak. If so, this may be a result of insufficient stress imposed on the ocean through ice movement or the lack of strong eddy formations along the shelf break in the model, either of which is likely to result in a larger transport offshore before the water gets to Barrow Canyon. It is also possible that the manner in which the model is forced at Bering Strait, with transport coming from the shelf break region in the eastern end of the domain, is influencing the shelf-interior exchange north of the Chukchi Sea.

[25] Although the focus of this study is on the Chukchi Sea, a brief overview of the offshore flow and deep circulation in the model is also in order. There is some exchange between the Chukchi Sea and the deep interior. There is approximately 0.22 Sv that flows northward from the central Chukchi Sea into deep water (deeper than 100 m) between the western boundary and Barrow Canyon. This transport is distributed over the water column, but the largest transports are found near the surface. The offshore transport decreases to 0.03 Sv, and is carried near the bottom, when the model is run without wind-forcing. The offshore flow below 50 m is essentially the same as for the standard wind-forced case, but the upper level velocity is greatly reduced, and even reversed slightly near the surface. The mean wind and ice drift have westward components, so the surface Ekman transport will have an offshore component. The offshore transport is due primarily to the upper layer Ekman transport with a much smaller contribution from the bottom boundary layer.

[26] The circulation in the Beaufort Sea is dominated by the anticyclonic Beaufort Gyre and a weaker cyclonic circulation near the Alaskan coast. The large-scale deep ocean circulation features are mainly wind-driven, although the smaller scale features are directly related to local topography. The mean wind curl from NCEP for the year 2000 shows the anticyclonic forcing that drives the Beaufort gyre (Figure 6). There is also a region of cyclonic wind curl along the northern Alaskan coast, coincident with the region of cyclonic circulation in the model. Calculations with no wind forcing do not produce the large-scale anticyclonic Beaufort gyre or the cyclonic circulation near the Alaskan coast, demonstrating that these features are wind-driven (although the artificial model boundaries are clearly influencing the Beaufort gyre). In a calculation with wind forcing in a domain extended eastward by 10° the cyclonic circulation is limited to the west of 140°W, very similar to the calculation shown here, so it is not limited by the presence of the solid eastern boundary but is instead

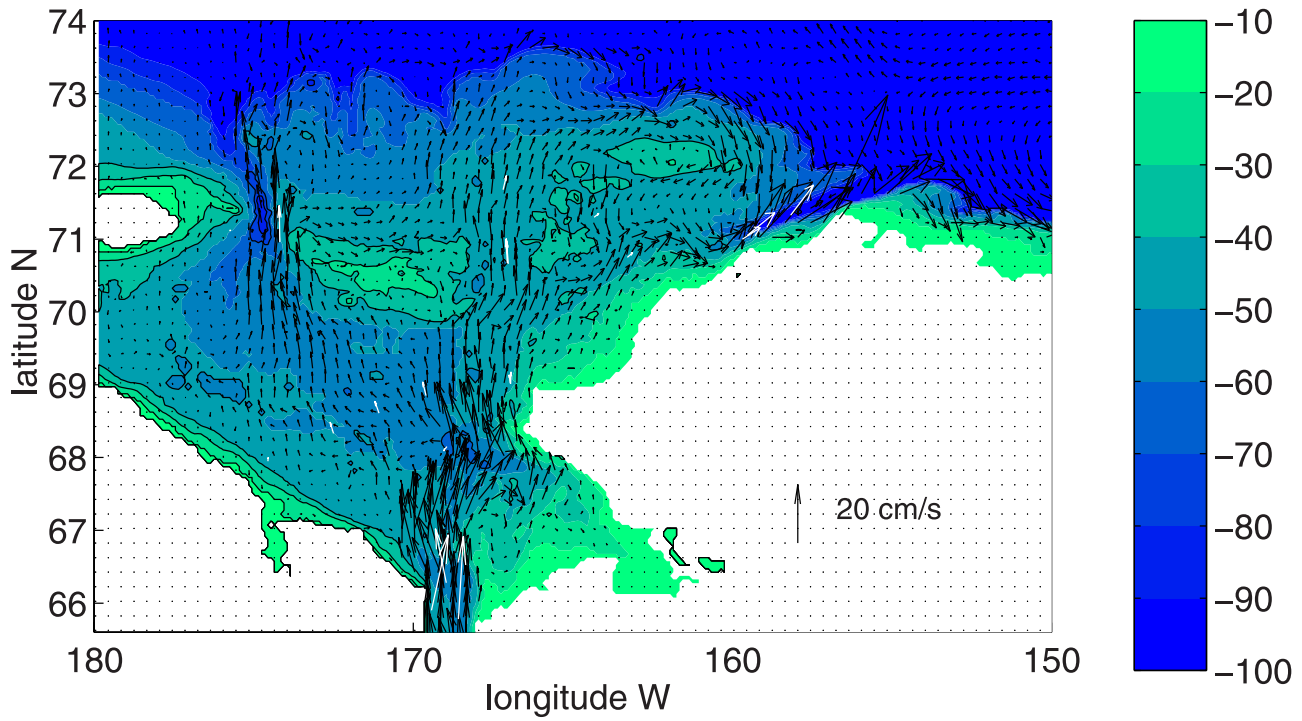

Figure 7. Annual mean horizontal velocity at 27.5 m depth (every fourth grid point) with the bottom topopgraphy. Mean velocities at various current meter sites (summarized in Table 1) are indicated by the white arrows.

coincident with the region of cyclonic wind curl. There is some indication that a cyclonic circulation exists in this region [*Toporkov*, 1970], but subsequent analysis in this study will focus on the Chukchi Sea.

[27] The annual mean velocity vectors (every fourth grid point) in the Chukchi Sea at 27.5 m depth from the final year of the wind-forced calculation are shown in Figure 7, along with the mean currents from various current meters (white vectors, summarized in Table 1). The general direction and magnitude of the mean velocities in the model agree well with the observations. Although the model velocity and the data are generally at different depths, the vertical shear of mean velocity at this depth is very weak. The mean model velocity just north of Bering Strait is $O(25\ \mathrm{cm\ s^{-1}})$, while the velocities in the interior of the Chukchi Sea are weaker, $O(5\ \mathrm{cm\ s^{-1}})$. The velocity in Herald Canyon is enhanced over that found in the interior due to the convergence of topographic contours and the tendency of the flow to follow the topography. The weak mean flow in regions of closed topographic contours and bays is evident. The convergence of the transport at the head of Barrow Canyon results in a narrow current with very strong velocities directed along the topography.

3.2. Temperature and Salinity

[28] The model temperature and salinity are now compared to mooring data in order to calibrate the model and determine the influence of Bering Strait inflow on the seasonal variability of temperature and salinity in the model. The model time series are taken from the model grid point closest to the location of the moorings. The data used are primarily from years 1990–1991 (W05b), as indicated in Table 1. The central Chukchi mooring MA3-93 from years 1993–1994 (dashed red line in the central Chukchi Sea) and upper Barrow Canyon mooring UBC3 (dashed red line in Barrow Canyon) are also used. The mooring data has been filtered with a boxcar filter of width 8 days. The model data is plotted every 4 days and has also been filtered with an 8 day boxcar filter. The model data are from the final year of integration, with the final 4 months of the year plotted at the beginning of the time series in order to match the data period of the moorings.

[29] Observations from 1990–1991 and 1991–1992 show the temperature in the central Chukchi Sea is at freezing from late in the year through early summer (Figure 8a). This timing is reproduced well in the model (black line). The warming in summer and fall is also found in the model, although the maximum temperature in the model is approximately 1.5°C warmer than in the observations. The salinity in the central Chukchi Sea is lowest in winter and a maximum in early spring (Figure 8b). The data in 1990–1991 are much saltier in winter than are the data in 1993–1994. The climatology of W05a shows that the winter of 1990–1991 had unusually high salinity in Bering Strait, the highest of their 14 year record. The model salinity compares very well with the data from 1993–1994 but, not surprisingly, is fresher than the data from 1990–1991. This fresh water bias in the model is seen at Herald and Barrow Canyons later in the year. The salinity maximum in late winter/early spring is reproduced well in the model, as is the gradual freshening later in the year. The salinity maximum in both the model and data is found approximately 1 month later than the salinity maximum at Bering Strait.

[30] A model calculation was also done that was forced with the seasonal cycle of temperature, salinity, and velocity at Bering Strait but had no ice model or surface forcing of

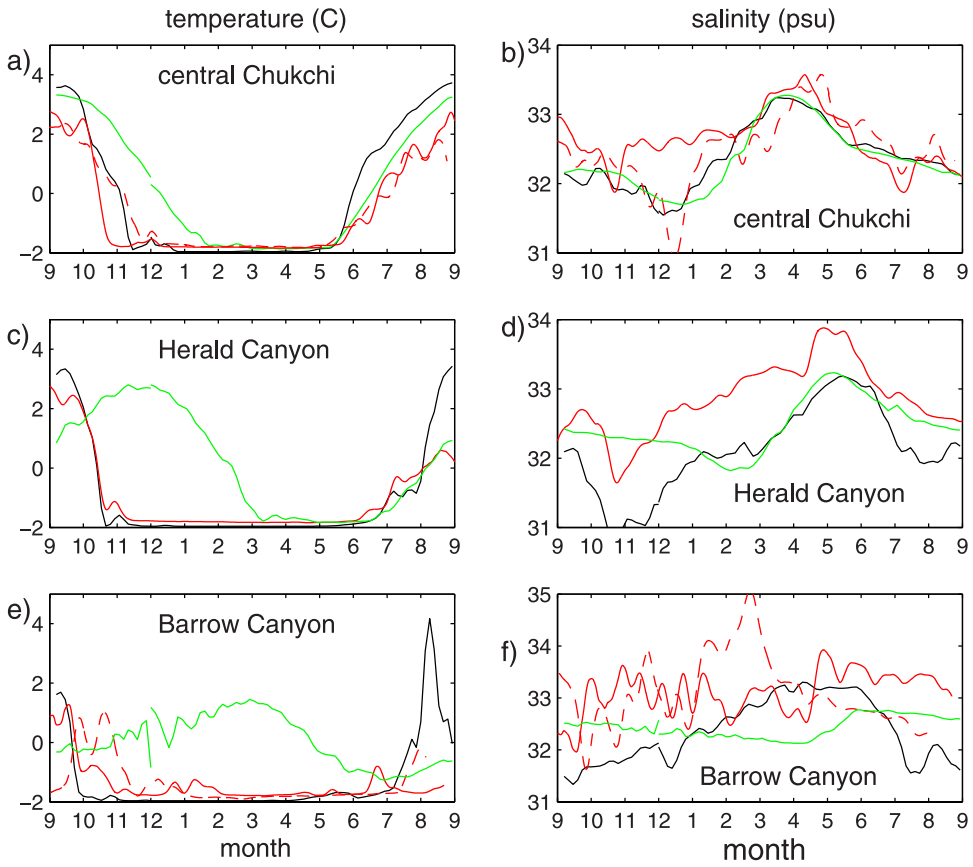

Figure 8. Time series of model temperature and salinity from the fully forced calculation (black lines) and from a calculation with full forcing at Bering Strait and no surface forcing or ice model (green lines) compared to mooring data from 1990–1991 (solid red line), 1993–1994 (dashed red line in central Chukchi Sea), and 1991–1992 (red dashed line in Barrow Canyon). The mooring locations and sources are indicated in Table 1, the model data are taken from the deepest level at each location.

any kind over the model domain (no flux of heat, fresh water, or momentum) (green line). The mean stream function for this case is very similar to that for the fully forced case. The Bering Strait transport is 0.82 Sv, with approximately 0.5 Sv going through Herald Canyon and 0.15 Sv going through the Central Channel and 0.15 Sv going along the coast of Alaska. This is to be compared with a distribution of 0.4 Sv, 0.2 Sv, and 0.2 Sv for the case with full forcing. This calculation provides an indication of how much of the variability at each location is a result of seasonal variability of temperature and salinity advected through Bering Strait. The unforced temperature and salinity in the central Chukchi Sea look much like that from the fully forced model runs, indicating that the low frequency variability of both temperature and salinity in this region is dominated by advection from Bering Strait.

[31] The timing of the freezing in winter and melt in fall is also reproduced well in the fully forced model at Herald Canyon (Figure 8c). The magnitude of the warm water compares well to the fall of 1990, but the model is more than 2°C warmer than the mooring data from the fall of 1991. This cooler water may be a result of cool inflow through Bering Strait in the summer of 1991 (data in W05a). The model calculation without surface forcing shows that the warm pulse found at Herald Canyon is not only due to advection from Bering Strait. The warm peak in the model with surface forcing arrives at Herald Canyon much earlier in the year than the water in the unforced calculation. This indicates that the water in the model was heated as it transited the Chukchi Sea and that the pulse of warmest inflow water was cooled before it reached Herald Canyon. The average temperature at this location for the unforced calculation is 0.2°C compared to −0.95°C for the forced model calculation and −0.89°C for the mooring data.

[32] The observed seasonal cycle in salinity at Herald Canyon is also found in the model, with the freshest water found in late fall and the saltiest water in early summer (Figure 8d). The data show a consistently higher salinity of approximately 0.5–1 psu than is found in the model. This is likely at least partially a result of the high salinity that was observed in Bering Strait and in the central Chukchi Sea a few months earlier, suggesting the importance of Bering Strait throughflow in setting the mean salinity. However, the salinity in the model is lower than that for the mooring over the entire year, while it is lower in the model only at some times of year at the other mooring locations. The lower salinity in the model may also be a result of insufficient ice formation. The timing and magnitudes of the increases and decreases in salinity are reproduced well in the model. The

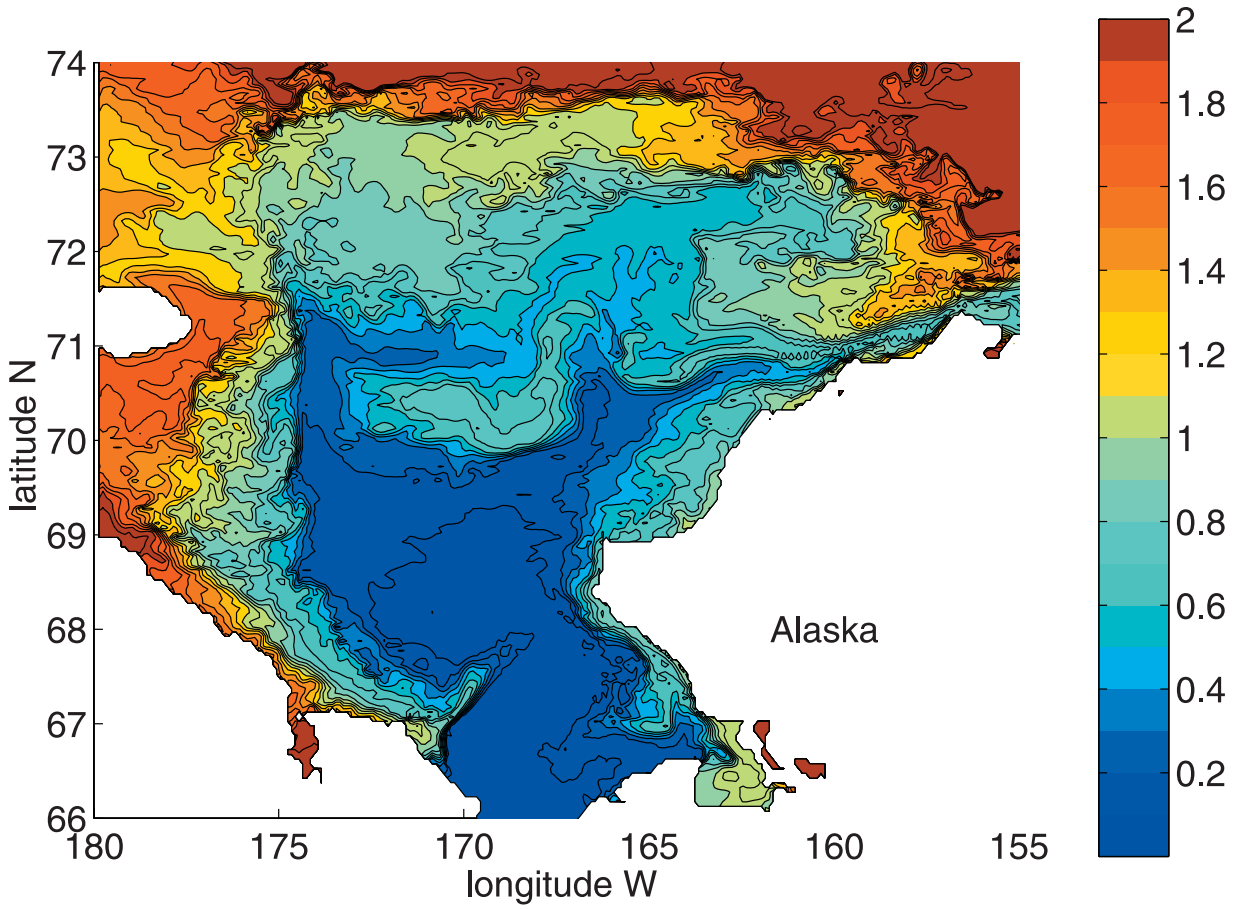

Figure 9. Age tracer at 27.5 m depth on model day 180 of year 3. This is a passive tracer that is initialized at zero throughout the domain, maintained at zero at Bering Strait, increases at a rate of 1 per year, and is advected, diffused, and mixed as temperature and salinity.

peak in salinity occurs a little later in the year than it does in the central Chukchi, once again suggesting an advective influence. The calculation without surface forcing does not show as much freshening in late fall, indicating that this is due in part to mixing downward of the low salinity surface waters with the onset of cooling, as suggested by W05b.

[33] The temperature signal at Barrow Canyon is dominated by freezing water for most of the year, with above freezing temperatures found in late summer and fall (Figure 8e). The model compares well with the fall of 1990 data, but is much warmer than the data from the fall of 1991. This is consistent with the bias found in the model at Herald Canyon. There are also several pulses of above freezing water in the winter that are seen in the mooring data but are not reproduced in the model. These events coincide with high salinity, indicating that they are a result of the warm, salty Atlantic water getting upwelled into Barrow Canyon (W05b). This is often observed and is thought to be driven by strong wind events and topographic waves [*Aagaard and Roach*, 1990]. It is not clear why the model does not produce such events. The model calculation without surface forcing shows the pulse of warm water that was introduced at Bering Strait in late summer arriving at Barrow Canyon in spring, a delay of approximately 6 months.

[34] The observed salinity signals at Barrow Canyon are not well reproduced in the model. There is a general increase in salinity in the model from fall through early summer, and a more rapid decrease in salinity from the end of summer into fall, as seen at each of the other mooring locations. The high salinity found in winter and spring is the model winter transformed water [*Weingartner et al.*, 1998]. There is a similar increase in salinity from fall to spring in the mooring data in each year, but it is punctuated by the high frequency, high salinity upwelling events throughout the winter months. The lower salinity in the model is partly due to the lack of upwelling events, but may also be related to the fresh bias found in the model at the other mooring locations and the dilution of the hypersaline waters by excessive mixing in the model. There is very little freshening observed in the fall of 1991, however the fall of 1992 shows a much larger decrease in salinity. The lack of freshening in the fall of 1991 is partly due to upwelling of Atlantic water in late July (W05b), but is also likely related to the high salinity inflow in the previous winter. The hypersaline water is dominant in the winter of 1991–1992 compared to the previous year. In summary, the model shows a clear seasonal cycle at Barrow Canyon that is not seen in the mooring data from 1990–1991. The data from 1991–1992 shows a similar freshening in the fall as is found in the model, but has much higher salinities in winter

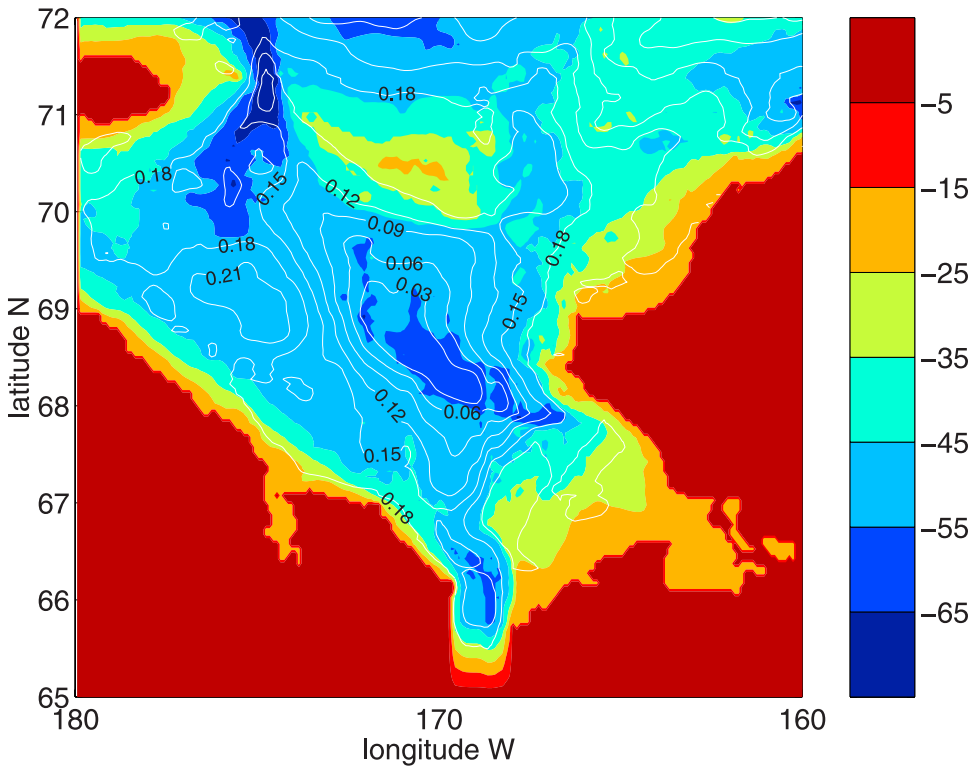

Figure 10. Mean transport stream function in the Chukchi Sea with Bering Strait closed for the final year (Sv, 1 Sv = 10^6 m^3 s^{-1}, white contours, contour interval 0.03) over bottom topography (m).

than in either 1990–1991 or the model. Clearly interannual variability is large, making evaluation of an annual repeat model calculation difficult.

[35] The forced model shows a much larger seasonal signal at Barrow Canyon than does the unforced model. The freshening in summer is a result of ice melt and advection, and the increase in salinity beginning in the fall is a result of ice formation and brine rejection. A model calculation with no seasonal cycle at Bering Strait, but with full NCEP surface forcing and the ice model, produces a salinity time series very similar to the calculation with seasonal variability at Bering Strait (not shown), indicating that in the model the forcing over the Chukchi Sea is important in determining the seasonal cycle in salinity flowing through Barrow Canyon. The maximum in salinity arrives earlier in the forced model than it does in the unforced model, suggesing that simple advection is no longer dominant.

[36] The final year of the model was also run with an inflow velocity determined by the local wind stress as v = 0.36 m s^{-1} + 0.04V_{wind}, as suggested by W05b, where v is the northward velocity in Bering Strait and V_{wind} is the NCEP 10 m meridional wind. This forcing results in mean transport through Bering Strait of 0.81 Sv and stronger high frequency variability of the inflow strength, including some reversals of the flow. However, the mean transport stream function, and low frequency variability of temperature and salinity, are very similar to those reported here.

4. Model Analysis

4.1. Residence Time

[37] The amount of time it takes for parcels to transit the Chukchi Sea is indicated by a passive tracer that is advected and diffused in the same way as temperature and salinity, but has no surface forcing, is initialized to zero everywhere, maintained at zero in Bering Strait, and increases linearly with time outside of Bering Strait (Figure 9). The main ventilation pathways across the Chukchi Sea are indicated by the bands of relatively young water extending from Bering Strait through Herald Canyon, Central Channel, and along the Alaskan coast. This field is on model day 180, in early summer when the transport through Bering Strait is near its maximum. The time since water parcels entered through Bering Strait is 1–3 months over most of the central Chukchi Sea. There is a sharp boundary along the western Hope Sea Valley, extending northward to Herald Canyon, between the recently ventilated waters coming from Bering Strait and those to the west of approximately 175°W. The waters over Herald Shoal are older, approximately 9 months. The water over Hannah Shoal is a mix of young and old water as the high frequency, small scale exchange is in the process of advecting water on and off the shoal. The water very near the east coast is older, particularly near 70°N, where the topography is shallow and not directly accessible by advection. As will be shown in section 4.5, this is where polynyas are formed. This old water gets flushed out of the region in the spring and summer months and is replaced by younger water again. This cycle in the model repeats each year. The water being transported eastward along Barrow Canyon is, on average, 6–8 months old, similar to the transit time found in the model of *Winsor and Chapman* [2004]. This represents a mix of waters that took a fairly direct route along the east coast and waters that took the longer, slower route through Herald Canyon and Central Channel, and turned eastward

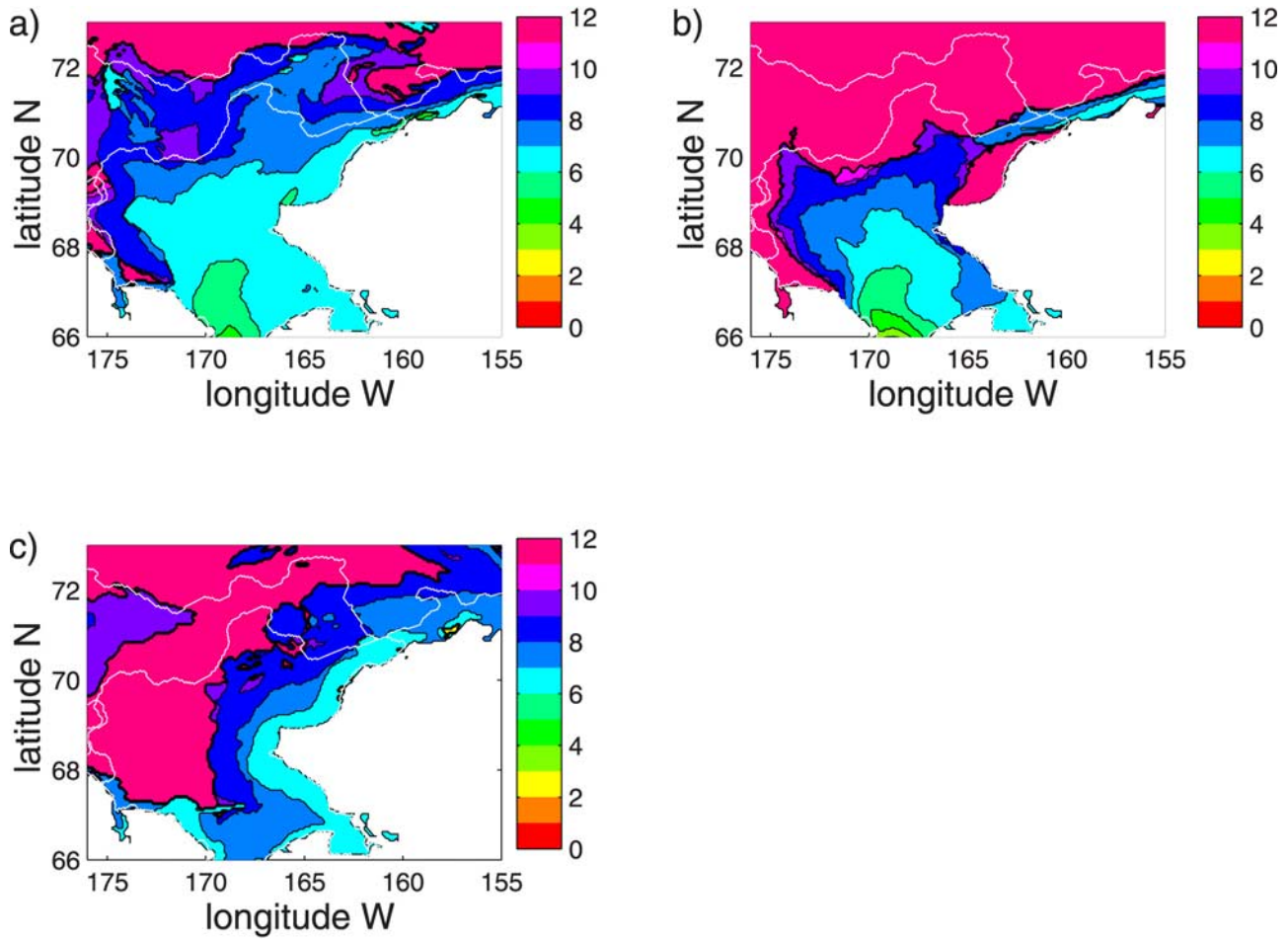

Figure 11. Month at which ice first melts in the model for (a) standard calculation, (b) monthly mean forcing, (c) no advection through Bering Strait. Results in (a) and (c) were forced with fluxes derived from daily NCEP fields. Regions indicated as 12 months are ice covered all year. The two white lines are the ice edge as inferred from QuikSCAT data on July 15 and August 15, 2000 (NASA SCP Arctic and Antarctic Ice Extent from QuikSCAT, 1999–2004, obtained from ftp://sidads.colorado.edu/pub/DATASETS/scatterometry).

along the shelf break, mixing with those trapped over the shoals. Using mooring data, W05b estimate the time for water parcels to cross the Chukchi Sea to either Herald Canyon or Barrow Canyon to be approximately 1–6 months. This is similar to that found in the model for Herald Canyon, but less than the average time found for Barrow Canyon.

4.2. Local Forcing of Mean Circulation

[38] The final year of the model calculation was also run by restarting the model at the end of the second year, but with Bering Strait closed off. The surface forcing is calculated using the daily NCEP fields, as for the standard calculation. The annual mean stream function over the Chukchi Sea is shown in Figure 10 (note the change in contour level). The circulation is much weaker, about 25% of the mean, and dominated by a cyclonic circulation of strength $O(0.2)$ Sv. This sense of circulation is in accord with the local annual mean wind stress curl (Figure 6). Most of this circulation is limited to the south of Herald Shoal, but approximately 0.04 Sv passes northward through the Central Channel and returns southward through Herald Canyon. The difference between the standard calculation and one with the Bering Strait inflow but no surface forcing looks very much like this result using surface forcing and no Bering Strait inflow, so that the influences of Bering Strait and local forcing on the mean transport stream function are approximately linear. This result indicates that the mean flow through the Chukchi Sea is dominated by the Bering Strait influence, and the local forcing acts primarily to induce a cyclonic circulation south of Herald Shoal.

4.3. Ice Melt

[39] The mean circulation northward from Bering Strait exerts a strong influence on the ice coverage in the Chukchi Sea. The month at which ice first melts in the model is shown in Figure 11a, the regions north of 72° that are indicated as 12 months are ice covered all year. There is a clear progression in the time at which ice first melts from Bering Strait northward. The ice melts in late spring/early summer over most of the southern Chukchi Sea. The influence of the bottom topography and advection by the

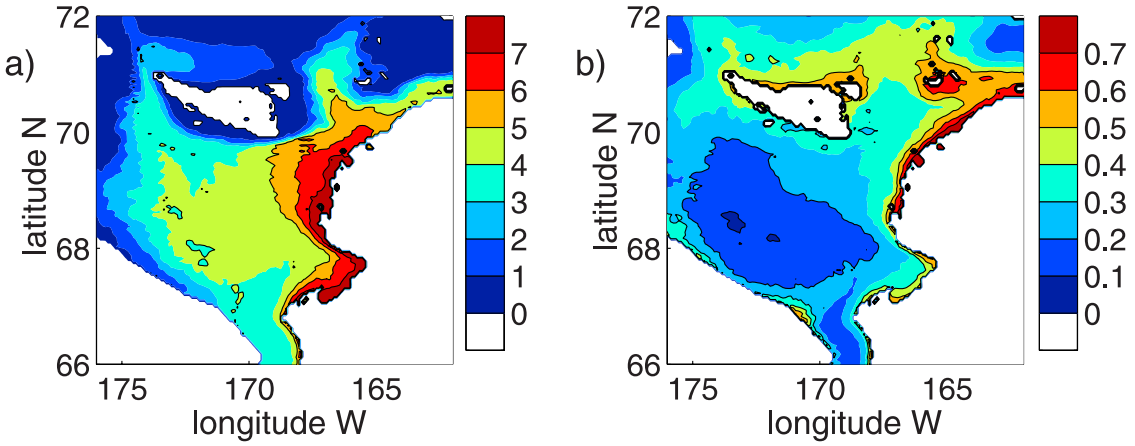

Figure 12. Variance in (a) temperature ($°C^2$) and (b) salinity (psu^2)at 42.5 m depth calculated over the final year of integration. White regions indicate land.

general circulation is evident by the delayed ice melt over Herald and Hannah Shoals. This pattern and timing of ice melt is consistent with the observations of *Bourke and Paquette* [1976] and *Martin and Drucker* [1997], who inferred that circulation over the shoals was weak as a result of conservation of potential vorticity by the mean flow. It is also generally consistent in pattern and timing with the passive age tracer in Figure 9.

[40] There is a general pattern of earlier ice melt near the Alaskan coast because heat advection in the ACC is strong and the model ice is not as thick at the beginning of the year as in the interior. Upwelling favorable wind events are also likely important. There is a tendency of delayed ice melt (and increasing thickness) towards the west. This is partly a result of the lack of advective influence from Bering Strait in this region, and the closed Long Strait, but is also a result of the wind-driven ice drift, which is generally from northeast to southwest over the Chukchi Sea in the model.

[41] The ice edge as inferred from QuikSCAT satellite data on July 15 and August 15, 2000 are indicated by the white lines, where the southernmost line is earlier in the year. The general trends found in the model are also observed in the data, particularly the rapid ice melt along the Alaskan coast and the delayed ice melt over Hannah and Herald Shoals. The observations also indicate delayed ice melt along the coast of Siberia, although this region in the model is likely influenced by the closed Long Strait. The observed ice edge continues to move northward later in the year, resulting in a maximum ice retreat that extends 100–200 km further northward than is found in the model. The main point here is not to accurately simulate the specifics of the ice edge, which will of course depend on conditions in the previous year that are not represented in the model (atmospheric forcing, ice cover, interannual variability at Bering Strait, etc.), but instead to demonstrate that the model is producing patterns and timing of ice melt that are in reasonable agreement with observations.

[42] A calculation with forcing derived from the monthly mean NCEP variables (restarted from the end of year 2 of the daily forced calculation) shows that the shoals and most of the northern Chukchi Sea remain ice covered all year long (Figure 11b), highlighting the importance of high frequency forcing and eddy fluxes in breaking up the ice and in enhancing exchange over the shoals. This result also indicates that the sensible heat flux, derived from the monthly mean NCEP air temperature that includes the

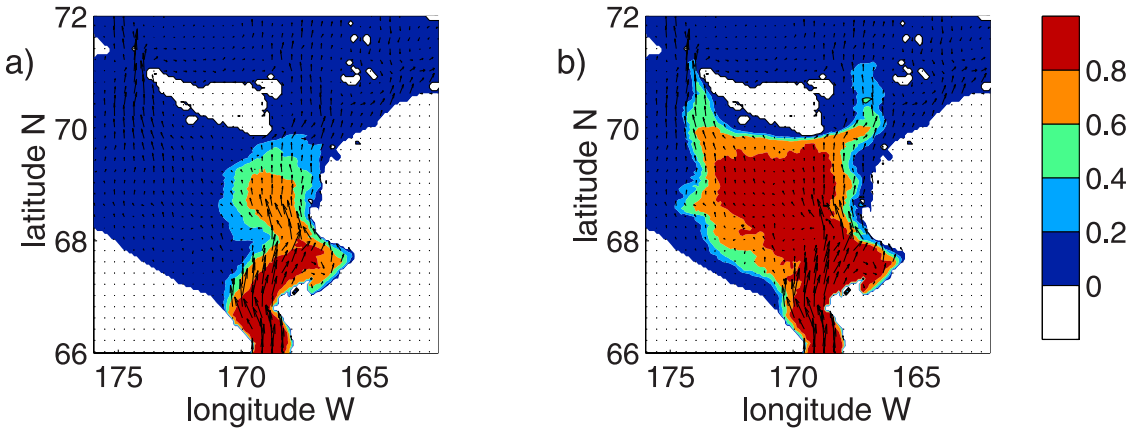

Figure 13. Amount of the variance in a) temperature and b) salinity at 42.5 m depth explained by a passive tracer with the same inflow boundary conditions and advection/diffusion/mixing but with no surface forcing, see equation (5). White regions indicate land.

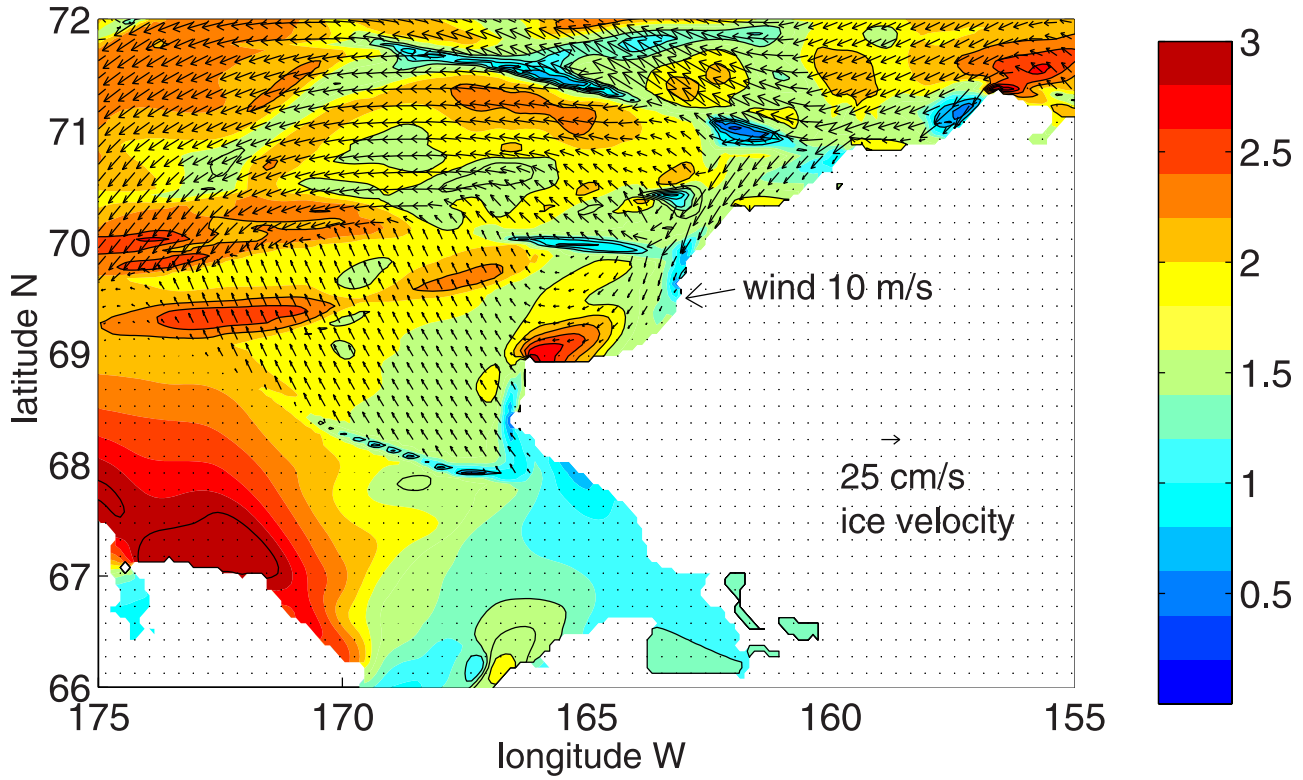

Figure 14. Ice thickness (m) and ice velocity on model day 64 (early March). The wind direction is indicated by the vector over land between Cape Lisburne and Point Barrow, a scale vector for the ice velocity is given over Alaska.

influence of the actual ice melt, is not sufficient to melt the ice over the shoals and that it must be a result of the resolved ocean circulation in the model.

[43] The importance of horizontal advection for the model ice melt is demonstrated by the calculation in which Bering Strait is closed for the final year (Figure 10), otherwise forced with surface fluxes derived from the daily NCEP fields, as in Figure 11a. The ice melt pattern in this case is quite different from either of the previous cases (Figure 11c). The delayed ice melt over Herald and Hannah Shoals no longer stands out. In fact, the ice melt even in the southern Chukchi Sea is much later in the year than is found when advection is present. The ice melts earliest near the Alaskan coast and the ice edge slowly progresses into the Chukchi Sea, reflecting the initial ice thickness at the beginning of the year. This result is not surprising, since heat advection has long been thought to be important for ice melt. However, it does demonstrate that the ice melt in the model is controlled by the ocean circulation and the model thermodynamics, and is not imposed by using the observed NCEP air temperature to derive the sensible surface heat flux. The NCEP product is produced on a roughly 2° grid, and does not resolve the fine scales of the advective pathways, so the spatial patterns in Figure 11a clearly must be coming from the model dynamics.

4.4. Regions of Bering Strait Influence

[44] The time series of temperature and salinity in section 3 suggest that the seasonal variability of salinity over much of the Chukchi Sea as far north as Herald Canyon can be related to that at Bering Strait, but that much of the temperature variability, and the salinity variability at Barrow Canyon, in the model are not simply related to that at Bering Strait. The variance of temperature and salinity in the model at 42.5 m depth calculated over the final year of integration are shown in Figure 12. The largest temperature variance is found near the Alaskan coast, with values exceeding 7°C^2. The variance rapidly decreases away from the coast but maintains values of approximately 4°C^2 over most of the central Chukchi Sea. The salinity variance is also a maximum near the Alaskan coast with values exceeding 0.7 psu^2. The salinity variance is also large in the shallow waters around Herald and Hannah Shoals. The lowest values of salinity variance are found in the central and southern Chukchi Sea, including the inflow through Bering Strait.

[45] Passive tracers have been integrated in the fully forced model calculation in order to better document the relative influences of local forcing within the Chukchi Sea and remote forcing through Bering Strait on the variance of water mass properties. These tracers are forced at Bering Strait, and initialized, advected, and diffused in the same way as temperature and salinity, but they are not forced at the surface. The difference between the passive tracers and the active temperature and salinity can be attributed to surface fluxes within the Chukchi Sea. A measure of the amount of the variance in temperature and salinity (ν_T, ν_S) at 42.5 m depth over the final year of integration that is

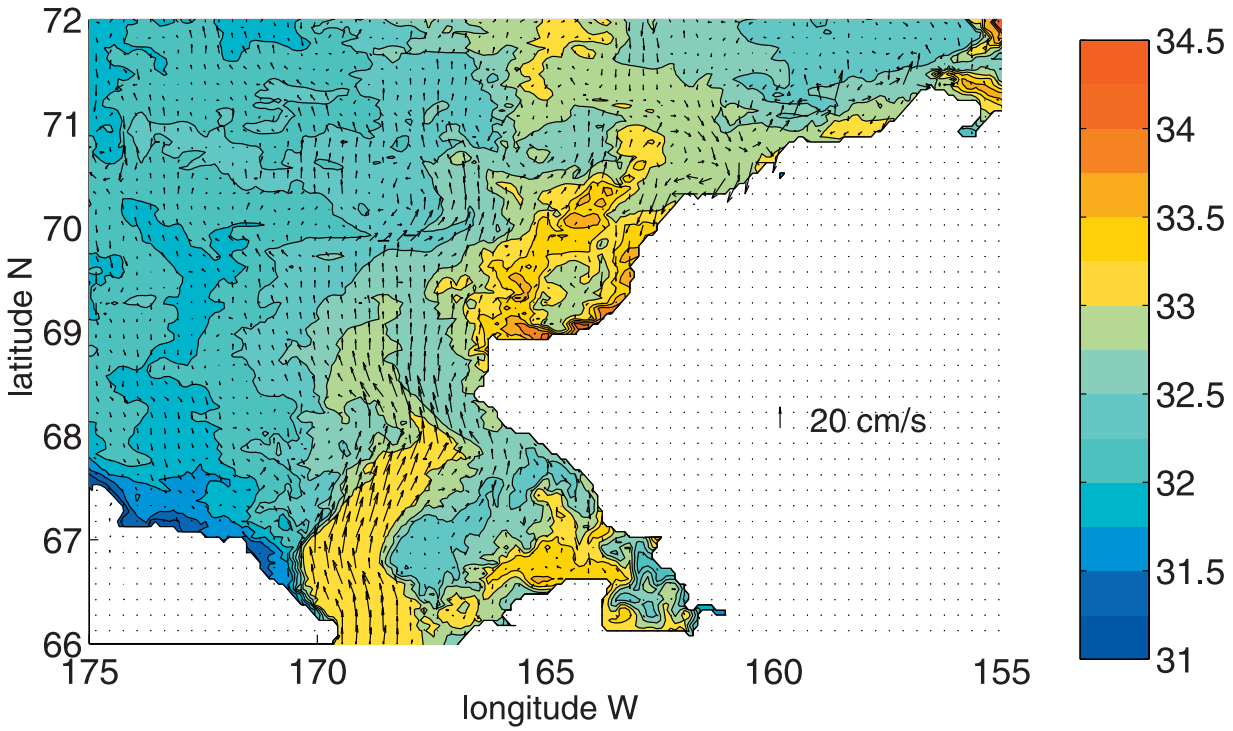

Figure 15. Bottom salinity (psu) and horizontal velocity (every 3 grid points) on model day 68, 4 days after the polynya event.

explained by the passive tracers is shown in Figure 13. This is calculated at each grid point for temperature as

$$\nu_T = 1 - \frac{\frac{1}{t_0}\int_0^{t_0} \left(P_T(x,y,t) - T(x,y,t)\right)^2 \, dt}{\frac{1}{t_0}\int_0^{t_0} \left(\overline{T}(x,y) - T(x,y,t)\right)^2 \, dt}, \qquad (5)$$

where T is temperature, $\overline{T}$ is the time mean temperature at each location, P_T is the passive temperature tracer, the integration time t_0 is one year, and data is provided every 4 days. If the passive tracer P_T is exactly equal to temperature, then $\nu_T = 1$. If P_T differs significantly from temperature, then ν_T becomes small. The difference is normalized by the standard variance of temperature at each grid point. Negative values of ν_T indicate that the difference between the passive tracer and temperature is, on average, greater than the temperature variance over the year. Since the main interest here is to identify those regions where P_T behaves like temperature, values of ν_T less than zero are set to zero.

[46] The general result is that little of the variability in temperature within the Chukchi Sea in the model can be explained by the transport through Bering Strait. Only within a fairly narrow band of O(50 km) width and O(250 km) length can a significant amount of the temperature variance be related to the inflow. In contrast, the variability in salinity over much of the southern Chukchi Sea (up to approximately 70°N) is driven by the seasonal cycle at Bering Strait. This is consistent with the general pattern of influence inferred from the mooring arrays in the southern and central Chukchi Sea by W05b, and is a consequence of a stronger surface forcing for heat flux than for fresh water flux. The calculation done with monthly mean values instead of every 4 days is very similar, so this result represents the dominant signal on seasonal timescales. The breakdown in the influence of Bering Strait on the variability of salinity occurs abruptly, coincident with Herald Shoal and Cape Lisburne. The shoal influence is clearly a result of topographic steering of the advective pathways. The breakdown near Cape Lisburne is instead coincident with the region of highest salinity variance and is related to polynya formations over shallow water in winter. Note that very little variability on seasonal and shorter timescales in the model north of Herald and Hanna Shoals, or at Barrow Canyon, is explained by the inflow at Bering Strait. Very low frequency variability (interannual and longer) will, however, be directly related to the salinity advected northward through Bering Strait.

[47] The seasonal salinity maximum in the model is produced in the central Chukchi Sea and as far north as Herald Canyon primarily by advection from Bering Strait. This is consistent with the conclusions of W05b based on mooring data from 1990–1991. The timing of the peaks in salinity in the model agrees well with that found in the data and suggests a fairly rapid propagation of 2–3 months for the high salinity signal to go from Bering Strait across the Chukchi Sea. This is also consistent with the conclusions of W05b and the age tracer in the model. The peak salinity is found at Barrow Canyon at a similar time lag from Bering Strait in both the model and in the observations of W05b and *Weingartner et al.* [1998]. However, the passive tracer revealed that it takes much longer, closer to 6 months, for water parcels to get from Bering Strait to Barrow Canyon. It should be noted that this is an average transit time, which reflects mixing in the model between older waters that

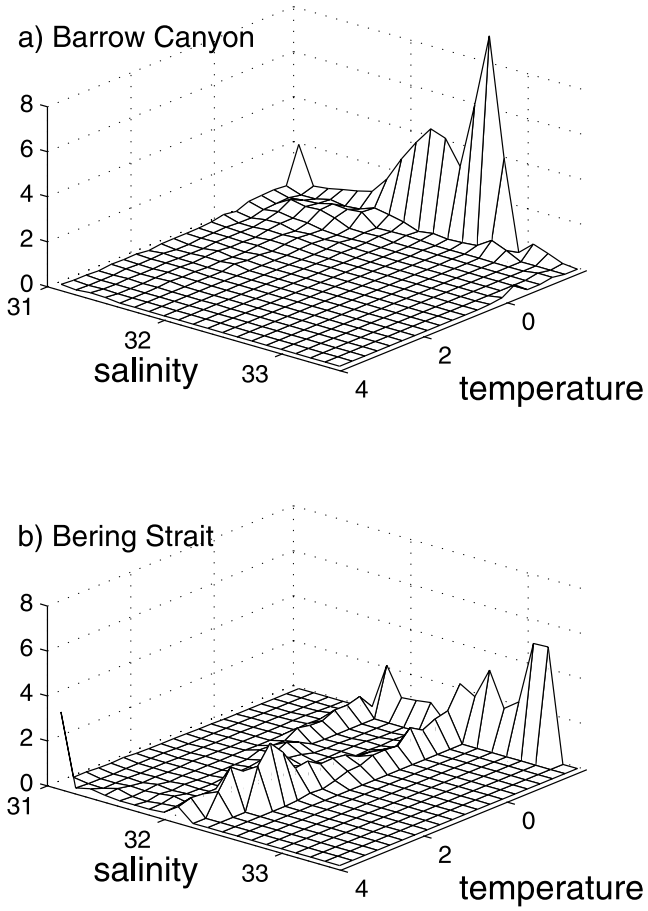

Figure 16. Annual mean transport weighted T/S census through a section at (a) 155°W, 71°N to 71.8°N and (b) Bering Strait between the surface and the bottom. The vertical axis is the volume transport through each section that has the indicated T/S properties (units 10^3 m^3 s^{-1}).

traveled from the northern Chukchi Sea and younger waters that took a more direct route along the Alaksan coast. Nonetheless, the model results suggest that the variance in the model is not simply advected there from Bering Strait.

[48] Consideration of a simple one-dimensional system suggests that this mismatch in the transit time between Bering Strait and Barrow Canyon inferred from the model salinity and that found in the model age tracer may be due to brine rejection along the advective pathway. For a one-dimensional flow with velocity V subject to forcing B, the salinity equation is written as

$$S_t = B - VS_y = -V^*\mathrm{Sy}, \tag{6}$$

where subscripts t and y refer to partial differentiation in time and space. $V^* = V - B/S_y$ is the effective velocity that would be inferred by following lines of constant S in time. The effective velocity is greater than the actual velocity when the forcing is of opposite sign to the meridional gradient in salinity. This is the case in the southern Chukchi Sea in winter when ice is being formed and salty water is being advected in from Bering Strait. This is also the case in summer when ice is melting and fresh water is being advected in through Bering Strait. A rough estimate of the apparent increase in advection speed is obtained by assuming that 1 m of ice is formed in 100 days over a water depth of 30 m, giving $B \approx 10^{-7}$ psu s^{-1}, and 1 psu change in salinity over 300 km, so that $V^* = V + 0.03$ m s^{-1}. This is comparable to the mean velocity in the central and northern Chukchi Sea. Although clearly very idealized, this scaling suggests that the apparent propagation of the high salinity signal is not due soley to the northward movement of the high salinity waters but is also influenced by local brine rejection within the Chukchi Sea.

[49] Note, however, that interannual variability in both the flow through Bering Strait, and in the surface forcing over the Chukchi Sea, will be important in determining the relative influences of local and remote forcing. The absolute value of the salinity outflowing at Barrow Canyon will also be directly related to the annual mean and interannual variability of the inflowing salinity at Bering Strait, as concluded by W05b.

4.5. Water Mass Transformation

[50] The seasonal cycle of water masses advected through Bering Strait, combined with the local surface forcing, ice formation and melt within the Chukchi Sea act to form identifiable water masses that exit the Chukchi Sea through Barrow Canyon [*Weingartner et al.*, 1998]. There are various classifications of these waters, but the focus here will be on the dominant modes with salinities near 32.5 psu and at the freezing point, hereafter referred to as winter water, and hypersaline waters with salinities in excess of 34 psu.

[51] The hypersaline mode discussed by *Weingartner et al.* [1998] is formed in the model along the Alaskan coast, as demonstrated by a polynya event between days 64 and 68 (early March). The ice thickness and ice velocity on day 64 are shown in Figure 14. The ice thickness is O(2 m) over most of the Chukchi Sea, and larger near the Siberian coast. There are, however, several bands of very thin ice both along the Alaskan coast and extending into the interior. The general direction of the ice drift is towards the west, away from the Alaskan coast. The wind is blowing towards the west southwest, as indicated by the arrow over land between Cape Lisburne and Point Barrow. The ice thickness divergence near the coast causes polynyas to form. As a result of this ice advection by the wind, the ice is thinnest just downwind (in the atmospheric wind sense), and thickest just upwind, of points in the coastline. Several such events are found along the section between Cape Lisburne and Point Barrow. These regions of thin ice are exposed to great heat loss at the surface, resulting in rapid ice formation and brine rejection.

[52] The impact of these brief polynya events on salinity is shown in Figure 15. The winds have forced a flow reversal along the coast, and salinities greater than 34 psu are generated in the vicinity of the polynyas. The influence of this and previous polynya events in this region is evident by the high salinity spreading away from the formation region in a patchy pattern extending towards the north. Although the model resolution is only marginal to resolve instabilities associated with the spread of dense water masses [*Chapman and Gawarkiewicz*, 1997], strong wind events after the polynya has ceased are also found to advect these high salinity waters offshore. The existence of this

local salinity maximum is unrelated to the Bering Strait inflow and its region of spreading corresponds closely with the region of enhanced salinity variance and is where the breakdown in the influence of inflowing salinity on salinity variance is found.

[53] The model also produces a mode water similar to the winter water of *Weingartner et al.* [1998], as indicated by the distribution in T/S space of waters flowing through Barrow Canyon (Figure 16a). The vertical axis is the volume flux of waters within each T/S bin (increments of 0.35°C and 0.125 psu). This distribution was calculated by a transport weighted estimate of the flow across a meridional section at the exit of Barrow Canyon (155°W between 71°N and 71.8°N) between the surface and the bottom. Nearly all of the outflowing shelf water is near the freezing point, and the dominant mode is at 32.7 psu. The extent to which the waters have been modified within the Chukchi Sea is indicated by a similar calculation applied to the inflow at Bering Strait (Figure 16b). The waters are broadly distributed in temperature space, with values exceeding 4°C. They are also broadly distributed in salinity, spanning values less than 31 psu and greater than 33 psu. This clearly indicates that, in the model, the water mass characteristics of the flow through Bering Strait are significantly modified within the Chukchi Sea before they reach Barrow Canyon.

5. Summary

[54] Many aspects of the mean circulation and seasonal variability in the Chukchi Sea are reproduced in a high resolution, baroclinic, regional coupled ice-ocean circulation model. The transport through Bering Strait follows three distinct branches across the Chukchi Sea through Herald Canyon, the Central Channel, and along the Alaskan coast, in general agreement with recent observational estimates. In the model, approximately 70% of the transport exits the Chukchi Sea through Barrow Canyon, the remaining 30% flows northward in the upper Ekman layer west of Barrow Canyon. Observational estimates suggest less transport through Barrow Canyon, although the cause of this disagreement is not clear. The pattern of ice melt in spring and summer reflects these advective pathways, consistent with satellite images of ice melt patterns, and supports the assertion by *Martin and Drucker* [1997] that conservation of potential vorticity by the large-scale flow steers the advective pathways around the shallow topographic features of Herald and Hannah Shoals. The model does a reasonably good job of reproducing the mean velocity and transports, and the seasonal cycle in temperature, salinity, and ice cover, when compared to observations over most of the Chukchi Sea. However, there are some differences between the model and observations at Barrow Canyon. The model produces a strong seasonal cycle in the salinity of the waters that exit the Chukchi Sea through Barrow Canyon, with the highest salinities found in spring and early summer. The peak salinity in the model is similar to that found in 1990–1991 by W05b, but the peak salinities in 1991–1992 are much higher (W98). Freshening is found in the model in the fall, similar to what was found at the other mooring locations and in the mooring data from 1991–1992. However, the mooring data from 1990–1991 instead maintains high salinities through the year, increasing by approximately 1 psu over the year long mooring deployment (W05b). Clearly the interannual variability in this region is large, and makes evaluation of the model seasonal cycle difficult. Although the model reproduces many of the observed characteristics of the general circulation in the Chukchi Sea, several shortcomings in the model are evident. The model does not reproduce the strong upwelling of Atlantic waters that are often observed in Barrow Canyon, is missing flow through Long Strait, and, although not discussed, does not form enough anticyclonic eddies along the shelf break that are often observed in the interior of the Arctic Ocean.

[55] Numerous additional model calculations and diagnostics were carried out in order to shed some light on the processes responsible for the seasonal cycle in water properties and ice melt in the model. Advection through Bering Strait is important for both the large-scale timing of ice melt and for smaller scale features such as the delayed ice melt over Herald and Hannah Shoals. High frequency forcing and the resulting exchange with the surrounding area, rather than mean advection or local seasonal heating, are responsible for ice melt over the shoals. The seasonal cycle in salinity of waters in the central Chukchi Sea, and as far north as Herald Canyon, is controlled by the seasonal cycle at Bering Strait. However, in the model the seasonal cycle in salinity north of Herald and Hannah Shoals, and in Barrow Canyon, are largely controlled by atmospheric forcing and ice cycles over the Chukchi Sea. The seasonal variation in temperature throughout most of the Chukchi Sea is much more strongly influenced by forcing within the Chukchi Sea than it is by advection through Bering Strait. However, the mean and interannual variability of the salinity advected through Bering Strait in the model has a direct impact on the salinities found throughout the Chukchi Sea.

[56] **Acknowledgments.** This material is based upon work supported by the National Science Foundation Office of Polar Programs under grant 0421904. Any opinions, findings, and conclusions or recommendations expressed in this material are those of the author and do not necessarily reflect the views of the National Science Foundation. This work has benefitted from discussions with Bob Pickart, Tom Weingartner, Rebecca Woodgate, and Knut Aagaard. Tom Weingartner provided transport estimates at Barrow Canyon and the UBC3 mooring data, and Rebecca Woodgate provided mooring data from 1990–1991 and 1993–1994. Comments and suggestions from two anonymous reviewers also helped to improve the presentation.

References

Aagaard, K., and A. T. Roach (1990), Arctic ocean-shelf exchange: Measurements in Barrow Canyon, *J. Geophys. Res.*, *95*, 18,163–18,175.

Bourke, R. H., and R. G. Paquette (1976), Atlantic water on the Chukchi shelf, *Geophys. Res. Lett.*, *3*, 629–632.

Chapman, D. C., and G. Gawarkiewicz (1997), Shallow convection and buoyancy equilibration in an idealized coastal polynya, *J. Phys. Oceanogr.*, *27*, 556–566.

Coachman, L. K., K. Aagaard, and R. B. Tripp (1975), *Bering Strait: The Regional Physical Oceanography*, Univ. of Wash. Press, Seattle.

Hibler, W. D., III (1979), A dynamic thermodynamic sea ice model, *J. Phys. Oceanogr.*, *9*, 815–846.

Hibler, W. D., III (1980), Modeling a variable thickness sea ice cover, *Mon. Weather Rev.*, *108*, 1943–1973.

Jackett, D. R., and T. J. McDougall (1995), Minimal adjustment of hydrographic profiles to achieve static stability, *J. Atmos. Oceanic Technol.*, *12*, 381–389.

Johnson, W. R. (1989), Current response to wind in the Chukchi Sea: A regional coastal upwelling event, *J. Geophys. Res.*, *94*, 2057–2064.

Large, W. G., and S. Pond (1981), Open ocean flux measurements in moderate to strong winds, *J. Phys. Oceanogr.*, *11*, 324–336.

Large, W. G., and S. Pond (1982), Sensible and latent heat flux measurements over the ocean, *J. Phys. Oceanogr.*, *12*, 464–482.

Large, W. G., J. C. McWilliams, and S. C. Doney (1994), Oceanic vertical mixing: a review and a model with a nonlocal boundary layer parameterization, *Rev. Geophys.*, *32*, 363–403.

Marshall, J., C. Hill, L. Perelman, and A. Adcroft (1997), Hydrostatic, quasi-hydrostatic, and nonhydrostatic ocean modeling, *J. Geophys. Res.*, *102*, 5733–5752.

Martin, S., and R. Drucker (1997), The effect of possible Taylor columns on the summer ice retreat in the Chukchi Sea, *J. Geophys. Res.*, *102*, 10,473–10,482.

Maslowski, W., and W. H. Lipscomb (2003), High resolution simulations of Arctic sea ice, 1979–1993, *Polar Res.*, *22*, 67–74.

Münchow, A., E. C. Carmack, and D. A. Huntley (2000), Synoptic density and velocity observations of slope waters in the Chukchi and East-Siberian Sea, *J. Geophys. Res.*, *105*, 14,103–14,119.

Overland, J. E., and A. T. Roach (1987), Northward flow in the Bering and Chukchi Seas, *J. Geophys. Res.*, *92*, 7097–7105.

Paquette, R. G., and R. H. Bourke (1974), Observations on the coastal current of arctic Alaska, *J. Mar. Res.*, *32*, 195–207.

Proshutinsky, A. (1986), Calculating surge fluctuations in the level and circulation of water of the Chukchi Sea, *Meteorol. Gidrologia*, *1*, 54–61.

Roach, A. T., K. Aagaard, C. H. Pease, S. A. Solo, T. Weingartner, V. Pavlov, and M. Kulakov (1995), Direct measurements of transport and water properties through the Bering Strait, *J. Geophys. Res.*, *100*, 18,443–18,457.

Spaulding, M., T. Isaji, D. Mendelsohn, and A. C. Turner (1987), Numerical simulation of wind-driven flow through the Bering Strait, *J. Phys. Oceanogr.*, *17*, 1799–1816.

Steele, M., R. Morley, and W. Ermold (2001), PHC: A global ocean hydrography with a high quality Arctic Ocean, *J. Clim.*, *14*, 2079–2087.

Toporkov, L. G. (1970), Nonperiodic currents, in *Soviet Arctic*, edited by I. P. Gerasimov, pp. 173–182, Nauka, Moscow.

Walsh, J. J., et al. (1989), Carbon and nitrogen cycling within the Bering/Chukchi Seas: Source regions for organic matter effecting AOU demands of the Arctic Ocean, *Prog. Oceanogr.*, *22*, 277–359.

Weingartner, T. J., D. J. Cavalieri, K. Aagaard, and Y. Sasaki (1998), Circulation, dense water formation, and outflow on the northeast Chukchi shelf, *J. Geophys. Res.*, *103*, 7647–7661.

Weingartner, T. J., K. Aagaard, R. Woodgate, S. Danielson, Y. Sasaki, and D. Cavalieri (2005), Circulation on the north central Chukchi Sea shelf, *Deep Sea Res., Part II*, *52*, 3150–3174.

Winsor, P., and D. C. Chapman (2004), Pathways of Pacific water across the Chukchi Sea: A numerical model study, *J. Geophys. Res.*, *109*, C03002, doi:10.1029/2003JC001962.

Woodgate, R. A., and K. Aagaard (2005), Revising the Bering Strait freshwater flux into the Arctic Ocean, *Geophys. Res. Lett.*, *32*, L02602, doi:10.1029/2004GL021747.

Woodgate, R. A., K. Aagaard, and T. Weingartner (2005a), Monthly temperature, salinity, and transport variability of the Bering Strait through flow, *Geophys. Res. Lett.*, *32*, L04601, doi:10.1029/2004GL021880.

Woodgate, R. A., K. Aagaard, and T. Weingartner (2005b), A year in the physical oceanography of the Chukchi Sea: Moored measurements from autumn 1990–1991, *Deep Sea Res., Part II*, *52*, 3116–3149.

Zhang, J., and D. A. Rothrock (2000), Modeling Arctic sea ice with an efficient plastic solution, *J. Geophys. Res.*, *105*, 3325–3338.

Zhang, J., W. D. Hibler III, M. Steele, and D. A. Rothrock (1998), Arctic ice-ocean modeling with and without climate restoring, *J. Phys. Oceanogr.*, *28*, 191–217.

M. A. Spall, Department of Physical Oceanography, Woods Hole Oceanographic Institution, Woods Hole, MA 02543, USA. (mspall@whoi.edu)